# Near-field visualization of focal depth modulation by step corrugated plasmonic slits

Baohua Jia,[1,a)] Haofei Shi,[2] Jiafang Li,[1] Yongqi Fu,[3] Chunlei Du,[2,a)] and Min Gu[1,a)]

[1]*Centre for Micro-Photonics and CUDOS, Faculty of Engineering and Industrial Sciences, Swinburne University of Technology, P.O. Box 218, Hawthorn, 3122 Victoria, Australia*
[2]*State Key Laboratory of Optical Technologies for Microfabrication, Institute of Optics and Electronics, Chinese Academy of Sciences, Chengdu, Sichuan Province 610209, People's Republic of China*
[3]*School of Physical Electronics, University of Electronic Science and Technology of China, Chengdu 610054, Sichuan Province, People's Republic of China*

Nanometric plasmonic slits with stepped corrugations have been designed and fabricated to achieve plasmonic focusing and focal depth modulation. A scanning near-field optical microscope is employed to directly visualize the transmitted light from the slits. The near-field and far-field two-dimensional images taken at different planes parallel to the slit surface unambiguously demonstrated the focusing effect of the nanoslits. Furthermore, by forming stepped corrugations with either a concave or a convex profile on both sides of the slits, the phase of the transmitted beam can be effectively manipulated, thus allowing an accurate tuning of the focal depth. © *2009 American Institute of Physics*. [DOI: 10.1063/1.3120542]

Since the extraordinary transmission was discovered in 1998,[1] the nanoplasmonics field has thrived rapidly by witnessing exponentially growing publications each year.[2–4] With the ability to manipulate light in nanoscale with great simplicity, nowadays nanoplasmonics has been redeemed as the solution for ultraminiaturized all-optical devices for a diverse range of applications including high resolution imaging, optical data storage, nanophotolithography, biosensing and chemical-sensing, quantum and atom optics, and telecommunications.[2–5] Among these applications, the intriguing lensing property of nanoplasmonic slits has made them extremely useful since electromagnetic (EM) field can be concentrated into a subwavelength spot by employing a simple groove surrounded nanometric slit milled in a thin metallic film.[6–8]

The general design of the plasmonic slit is shown in Fig. 1(a). When a TM polarized (magnetic field parallel to the *y* direction) monochromatic plane wave impinges on the slit, it excites collective oscillations of the electrons at the surface, which is known as surface plasmon polaritons (SPPs). The SPPs propagate along the surface of the metal film and are diffracted to the far-field by the periodic grooves.[9] Constructing interference of such diffracted beams leads to the focusing effect at a certain point on the beam axis.[10] Since the diffracted beams are modulated by the nanometric grooves, through adjusting the parameters of the grooves (such as their width, depth, period, and number), the diffracted beams can be fully manipulated resulting in a tailored ultracompact lens with subwavelength resolution and nanometer accuracy.[6,11] Most interestingly, it has been numerically found[12] that the relative phase at the exit end of the slit increases steadily with the increasing groove depth, making it possible to achieve continuous phase retardation by simply designing surrounding grooves with stepped depths, as shown in Figs. 1(a) and 1(b). This has led to a great simpli-

fication of the plasmonic lens design without increasing the groove number or generating a bump on the metal film.[13]

In this paper, step corrugated plasmonic slits were fabricated and their functionalities have been rigorously examined by a scanning near-field optical microscope (SNOM). Compared with the far-field characterization techniques such as using a charge coupled device,[10] SNOM offers resolution down to a nanometer scale, which is far beyond the diffraction limit and is essential for characterizing nanoplasmonic devices.[14,15] In the SNOM measurement, both near-field and far-field intensity distributions at different planes vertical to the optical axis have been obtained and compared with simulation results using the finite difference time domain (FDTD) method. It has unambiguously revealed that the transmitted light has been effectively focused by the nanoslits. With a change in the height of the nanocorrugations in a stepped
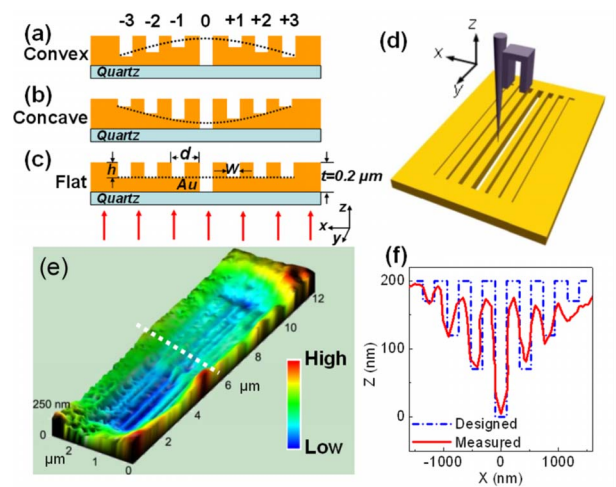


FIG. 1. (Color online) Schematic drawing of the nanoplasmonic slits with (a) convex, (b) concave, and (c) flat shaped profiles. (d) Schematic drawing of near-field measurement setup. (e) Measured topographic image of the slit with concave corrugations. (f) Cross section of the concave groove-slit at the position indicated by the dashed line in (e).

a)Authors to whom correspondence should be addressed: Electronic addresses: bjia@swin.edu.au, cldu@ioe.ac.cn, and mgu@swin.edu.au.

TABLE I. Design parameters of the three types of nanoplasmonic slits.

| Type | Flat | Concave | Convex |
|---|---|---|---|
| Film thickness ($t$) | | 200 nm | |
| Slit and groove length | | 10 $\mu$m | |
| Slit and groove width ($w$) | | 200 nm | |
| Slit and groove period ($d$) | | 420 nm | |
| Height of slit ($h$) | | 200 nm | |
| Height of groove 1 and $-1$ | 80 nm | 130 nm | 30 nm |
| Height of groove 2 and $-2$ | 80 nm | 80 nm | 80 nm |
| Height of groove 3 and $-3$ | 80 nm | 30 nm | 130 nm |

manner, the transmitted beam has been focused with different focal depths, suggesting that the plasmonic lenses function well as designed and thus the manipulation of focal depth through phase control has been experimentally demonstrated.

As shown in Fig. 1, to examine the phase control properties three types of slits have been designed and fabricated in a 200-nm thick gold film on a quartz substrate using focused ion beam milling.[16] The "flat" type is formed by milling a 200 nm wide slit surrounded by grooves with the same height ($h=80$ nm). The periodicity and width of the grooves are $d=420$ nm and $w=200$ nm, respectively. The length of the slit and grooves are 10 $\mu$m. The design of the "concave" or "convex" type is exactly the same as that of the flat one, except that the height of individual groove is different so that they form either a concave or a convex profile analogous to the profile of a conventional lens. The detailed parameters of the three types are presented in Table I.

To characterize the functionalities of the slits, a SNOM (Solver, NT-MDT) was employed. The SNOM setup is the same as the one used in our previous experiment,[17] except that the light source is a TM-polarized collimated helium-neon laser ($\lambda=632.8$ nm). As illustrated in Fig. 1(d), the scanning probe is the core element of the system. During the experiment, the topographic signals and the optical signals were acquired simultaneously all the time to allow a correlation between them. Figure 1(e) presents the three-dimensional topographic image of the concave slit. A cross section of it [Fig. 1(f)] clearly shows the depth difference of the grooves on both sides of the slit, which matches well with the design.

The measured intensity distributions of the transmitted light at different planes parallel to the flat type slit plane are presented in Fig. 2. At a plane approximately 10 nm away from the surface, strong optical signals with a width of roughly 200 nm and a length of approximately 10 $\mu$m reproducing the morphological profile of the slit can be observed. Since the film thickness (200 nm) is several times larger than the skin depth of gold [$\sim$20 $\mu$m at 632.8 nm (Ref. 18)], the observed high contrast signals are solely resulted from the excitation of SPPs rather than the interference with directly transmitted light.[15] Besides this strong signal in the center, a low intensity region with an area of $\sim1.7\times10$ $\mu$m$^2$ can also be observed on both sides of the slit, which clearly demonstrates the propagation of the excited SPPs along the incident polarization direction.

Figure 3(a) presents a detailed comparison of the measured intensity distributions with simulations using FDTD at the slit cross section [along the $X$ direction, as indicated by
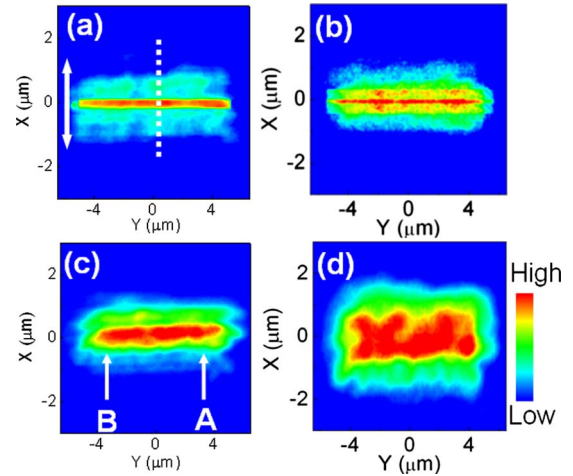


FIG. 2. (Color online) Intensity distributions of transmitted light through the flat slit at planes with distance at (a) $z=10$ nm, (b) $z=50$ nm, (c) $z=1600$ nm, and (d) $z=4000$ nm to the slit surface. The arrow in (a) indicates the incident polarization direction.

the white dotted line in Fig. 2(a)]. A good agreement has been found between the experiment and the theoretical prediction except that the measured full width at half maximum (FWHM) of the central lobe (approximately 281 nm) is slightly larger than the calculated value of 230 nm. This is because the measured intensity distribution is approximately the convolution of the finite probe size (30–80 nm) and the actual intensity distribution of the transmitted light.[19]

When the probe was withdrawn from the interface, the measured intensity decreased rapidly due to the fast decaying nature of the EM field of SPPs in the direction vertical to the slit interface. In the mean time interesting interference patterns started to emerge. For example, as shown in Fig. 2(b) at a plane about 50 nm away from the interface, the light field exhibits a strong and narrow central lobe surrounded by two thin strong side lobes. The nanometric fine features presented in this figure clearly demonstrates the interaction of SPPs with the nanostructures in the near-field region, which was not previously accessible with the far-field measurement.[10] A comparison of the measured cross section with the FDTD
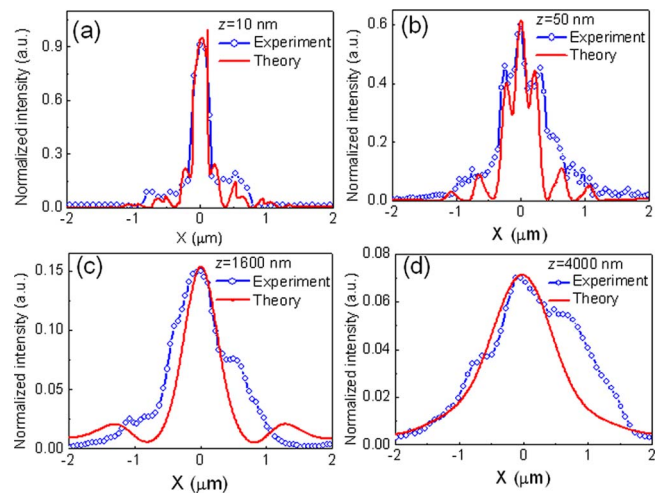


FIG. 3. (Color online) Comparison of measured and theoretical cross sections at $Y=0$ in Fig. 2 for (a) $z=10$ nm, (b) $z=50$ nm, (c) $z=1600$ nm, and (d) $z=4000$ nm.
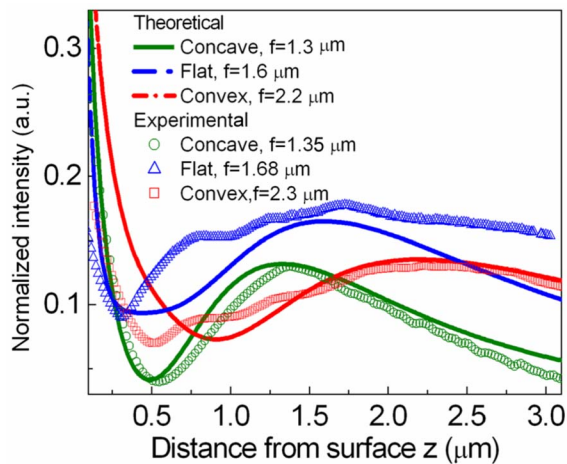
FIG. 4. (Color online) Comparison of the measured (dotted curves) and the theoretical (solid curves) focal depths for three types of slits (flat, concave, and convex).

simulation in Fig. 3(b) reveals that the observation agrees well with the theory.

The focusing property of the plasmonic lens is examined by mapping the intensity distribution at a $z=1600$ nm plane where the focusing effect is theoretically expected. As shown in Fig. 2(c), a strong concentrated intensity distribution was observed. The measured cross section profile in Fig. 3(c) agrees reasonably well with the calculation with a slightly larger FWHM in experiment (850 nm) than that calculated (620 nm). This is due to the measured plane at $z=1600$ nm, which is not necessarily the actual focal plane of the slit in experiment. This has been confirmed by the focal depth measurement presented later in this paper. It can be noticed that the intensity distribution [Fig. 2(c)] along the $Y$ direction shows unexpected nonuniform FWHM from the symmetric design of the slit and grooves. This can be attributed to the structural defects of the groove-slit, which have been confirmed by the topographic image measured simultaneously. The marked area "A" clearly shows a large overall depth than that of the area "B." As a result, the generated phase retardation along the slit axis is nonuniform, which directly leads to the observed asymmetric intensity distribution in the focal plane. However, even with the presence of the imperfection, the focusing effect is obvious.

Figure 2(d) presents the far-field intensity distribution at a plane 4 $\mu$m away from the interface. At such a distance, the detected peak intensity significantly reduced to less than 7% of the intensity at the slit surface. The intensity distribution also shows a Gaussian shaped cross section but with a much larger FWHM ($\sim$1.5 $\mu$m) and a much lower peak intensity compared with that in Fig. 2(c).

Similar intensity distributions were also observed in the cases of concave and convex slits. To examine the ability to modulate the focal length, the transmitted optical signals were measured as a function of the distance to the interface for the three designs. As presented in Fig. 4, the measured focal lengths (distance from $z=0$ to the second peak of the curves) for concave, flat, and convex slits are approximately 1.35, 1.68, and 2.3 $\mu$m, respectively, agreeing well with the

calculated focal depths of 1.3, 1.6, and 2.2 $\mu$m, thus demonstrating the efficient tuning of the focal depth through modulating the exit phase of the transmitted beam from the slits. The measured smallest spot size of 603 nm in FWHM (along the $X$ axis) was achieved in the concave case after deconvolving the probe function, demonstrating that subwavelength resolution has been obtained. Moreover, a peak intensity comparison shows that at least more than 15% transmitted energy has been concentrated in the focal region, validating the high efficient groove-slit design in terms of diffracting SPPs.

In conclusion, three types of plasmonic slits with different stepped grooves have been designed and fabricated to achieve efficient plasmonic focusing and focal depth modulation of the transmitted beam. Near-field measurement reveals unambiguously the light interaction with the slits and confirms the functionalities of the nanoplasmonic lens. The simple plasmonic lens demonstrated in this paper can find broad applications in ultracompact photonic chips particularly for biosensing and high-resolution imaging.

[1] T. W. Ebbesen, H. J. Lezec, H. F. Ghaemi, T. Thio, and P. A. Wolff, Nature (London) **391**, 667 (1998).
[2] E. Altewischer, M. P. Van Exter, and J. P. Woerdman, Nature (London) **418**, 304 (2002).
[3] W. L. Barnes, A. Dereux, and T. W. Ebbesen, Nature (London) **424**, 824 (2003).
[4] S. I. Bozhevolnyi, V. S. Volkov, E. Devaux, J. Y. Laluet, and T. W. Ebbesen, Nature (London) **440**, 508 (2006).
[5] W. Srituravanich, L. Pan, Y. Wang, C. Sun, D. B. Bogy, and X. Zhang, Nat. Nanotechnol. **3**, 733 (2008).
[6] F. J. Garcia-Vidal, L. Martin-Moreno, H. J. Lezec, and T. W. Ebbesen, Appl. Phys. Lett. **83**, 4500 (2003).
[7] R. Yang, M. A. G. Abushagur, and Z. Lu, Opt. Express **16**, 20142 (2008).
[8] Z. Liu, J. M. Steele, H. Lee, and X. Zhang, Appl. Phys. Lett. **88**, 171108 (2006).
[9] Y. Xie, A. R. Zakharian, J. V. Moloney, and M. Mansuripur, Opt. Express **12**, 6106 (2004).
[10] L. B. Yu, D. Z. Lin, Y. C. Chen, Y. C. Chang, K. T. Huang, J. W. Liaw, J. T. Yeh, J. M. Liu, C. S. Yeh, and C. K. Lee, Phys. Rev. B **71**, 041405 (2005).
[11] B. Ung and Y. Sheng, Opt. Express **16**, 9073 (2008).
[12] H. Shi, C. Du, and X. Luo, Appl. Phys. Lett. **91**, 093111 (2007).
[13] Z. Sun and H. K. Kim, Appl. Phys. Lett. **85**, 642 (2004).
[14] H. Gao, J. Henzie, and T. W. Odom, Nano Lett. **6**, 2104 (2006).
[15] L. Yin, V. K. Vlasko-Vlasov, A. Rydh, J. Pearson, U. Welp, S. H. Chang, S. K. Gray, G. C. Schatz, D. B. Brown, and C. W. Kimball, Appl. Phys. Lett. **85**, 467 (2004).
[16] Y. Fu, W. Zhou, L. E. N. Lim, C. Du, X. Luo, Z. Zhao, X. Dong, H. Shi, and C. T. Wang, Opt. Eng. **45**, 108001 (2006).
[17] B. Jia, A. H. Norton, J. Li, A. Rahmani, A. A. Asatryan, L. C. Botten, and M. Gu, Opt. Lett. **33**, 1093 (2008).
[18] J. R. Reitz, F. J. Milford, and R. W. Christy, *Foundations of Electromagnetic Theory*, 4th ed. (Addison-Wesley, Reading, 1993).
[19] B. Jia, X. Gan, and M. Gu, Appl. Phys. Lett. **86**, 131110 (2005).